COBEM 2021 26th International Congress of Mechanical Engineering
November 22-26, 2021, Virtual Congress, Brazil
ABCM Associação Brasileira de Engenharia e Ciências Mecânicas

# COB-2021-1627
# ANALYSIS AND MODELING OF THE DYNAMIC BEHAVIOR OF CYLINDRICAL CABLES UNDER TRANSIENT EXCITATION

**Marcos Fabrício de Souza Aleixo Filho**
**Francisco Ricardo Cunha**
University of Brasília, Faculty of Technology, Department of Mechanical Engineering, Fluid Mechanics of Complex Flows Group - VORTEX, Brasília, Brazil
mffilhoaleixo@gmail.com
frcunha2@gmail.com

**José Alexander Araújo**
**Remy Kalombo Badibanga**
University of Brasília, Faculty of Technology, Department of Mechanical Engineering, Fatigue, Fracture and Materials Group - GFFM, Brasília, Brazil
jaaunb@gmail.com
badibanga12@gmail.com

***Abstract.*** *The present work brings a theoretical investigation of vortex-induced vibration, a phenomenon that commonly occurs in cylindrical bodies subjected to wind, such as aerial cables in power transmission lines. Mathematical models are proposed in order to predict the oscillatory motion of a cylindrical cable undergoing a wind current. In this paper we use: (i) a Duffing type model nonlinearharmonic oscillator; (ii) a concentrated model of a prototype cylinder suspended by nonlinear springs and forcing by a transverse flow; (iii) and the vibrating cylinder cable model. When the nondimensional physical parameter of the oscillatory system is much smaller than unity, a perturbation method provides an asymptotic solution for the prototype cable displacement. An excellent agreement is observed between the asymptotic and numerical solutions based on a standard Runge-Kutta algorithm. A dynamic analysis is presented for the nonlinear oscillator by using phase-space diagrams and amplitude-frequency plots, and by exploring the chaotic response of the system for nonlinear regimes with high amplitudes of excitation. In addition, experiments with a real transmission cable undergoing harmonic oscillations are carried out in order to measure the time-response at different longitudinal positions. When adjusting the system parameters of the theoretical model for the real values of the experiments, the nonlinear harmonic oscillator successfully fits the experimental data. For appropriate condition of damping and excitation, and after few manipulations, the concentrated cylinder model is seen to be equivalent to the nonlinear harmonic oscillator model. Finally, the vibrating motion of the prototype cylindrical cable is examined. From a scaling analysis of the nondimensional second order partial differential governing equation of the cable motion in space-time, the equivalence and consistency between the continuous and the concentrated models are demonstrated. We show that for small values of tensions applied to the cable, the wave propagation velocity is sufficiently small, and consequently the space second derivative along the length of the cable is only a weak contribution, resulting in a concentrated mass-spring-damper system.*

***Keywords:*** *conductive cables, wind vibration, Von Kárman vortex shedding, perturbation method, concentrated models.*

## 1. INTRODUCTION

The vortex wake formed in a laminar flow around structures with a circular cross section, such as cylinders and cables, cause cyclical forcing due to the periodic formation of vortices, whose circulation is alternately clockwise and counterclockwise. The pressure gradients generated by the periodicity of the vortex shedding induce, on the body, a harmonic forcing perpendicular to the flow direction.

One of the main focuses for investigating this fluid flow-structure interaction is to control the phenomenon of resonance and consequently the collapse of structures. When the vortex shedding frequency equals the natural frequency of the cylinder, or other circular section body, the peak-to-peak oscillation amplitudes reach their maximum. In the specific case of electric power transmission cables, when this occurs, the efforts on the structure are greater and the fatigue fracture process worsens, especially in the areas of attachment to the transmission poles or towers (Den Hartog, 1972). Also, as cables are continuous systems, they have a range of natural frequencies that are easily reached, since they are very close to each other, varying every 0.2 and 0.5 Hz (Guerard *et al.*, 2011).

This phenomenon was studied by Von Kárman, using dimensional analysis in a vibrating cylinder (Batchelor, 2000),

through which a relationship was verified between the angular frequency of vortex shedding $\omega_s$, the radius of the cylinder $d$ and the flow velocity $U$, given by the nondimensional Strouhal number

$$Sh = \frac{\omega_s d}{U}, \tag{1}$$

that denotes a physical parameter of dynamical system measuring the relative importance between the convection time scale of the flow and the vortex shedding frequency scale.

In the present work, we examine the dynamics of oscillations of a power transmission cable through concentrated models. We shall show that this model describe very well the oscillatory response along the time at a point of the conductor. Firstly, a purely dynamic model of a nonlinear harmonic oscillator is studied, whose parameters are further adjusted to generate responses similar to those observed experimentally through a test of real conductor cable on a bench. Secondly, we propose a concentrated model of a cylindrical cable undergoing an eolian excitation. Finally a complete space-time model of a vibrating cable is proposed and verified that in the asymptotic limit of small traction along the cable, the full space-time model reduces to a concentrated model of a cylindrical cable as the same properties of the cable are considered in both models.

## 2. Nonlinear harmonic oscillator

The first model proposed in this work in order to examine the dynamic of cable oscillation in a specific point is the nolinear harmonic oscillator of Duffing type (Logan, 2013), which have an elastic restitution coefficient nonlinear, given by

$$k^* = k(1 + \frac{a}{k}y^2), \tag{2}$$

where $a$ is a system constant, whether is big, brings a strong nonlinearity to the dynamic system. Take into account the damping effect, the governing motion equation can be expressed as follows:

$$m\frac{d^2y}{dt^2} + C\frac{dy}{dt} + k^*y = B\sin(\omega t), \qquad t > 0, \tag{3}$$

being $m$ the system mass, $C$ the damping coefficient and $B$ the amplitude excitation. Considering the initial condition $y(0) = A$ and $dy(0)/dt = 0$, it is possible to make Eq. (3) nondimensional using the following characteristic scales:

$$u = \frac{y}{A}; \quad t^* = t\omega_n, \tag{4}$$

where $\omega_n = \sqrt{k/m}$ is the non-damping natural frequency of the system. After few manipulations, the nondimensional governing equation stands as follows:

$$\begin{cases} \ddot{u} + 2\zeta\dot{u} + u = \beta\sin(\omega^* t^*) - \varepsilon u^3, & t^* > 0, \\ u(0) = 1, \qquad \dot{u}(0) = 0. \end{cases} \tag{5}$$

where $2\zeta = C/m\omega_n$ and $\beta = B/kA$ are the nondimensional damping and amplitude coefficients, respectively. Here, $\varepsilon$ is a nondimensional parameter that defines the degree of nolinearity of the solution, namely:

$$\varepsilon = \frac{A^2 a}{k}. \tag{6}$$

The advantage of this model is its completeness the meaning that it is possible to capture solutions from linear to nonlinear regimes just by adjusting the physical parameters. Using a fourth order Runge-Kutta algorithm with a typical time step of 0.01 we can compute the numerical solution of differential Eq. (5) for an arbitrary values of $\varepsilon$. We shall show plots of displacement of the cable as a function of time as well as the solution trajectory of the dynamic system in the phase diagram (i.e. velocity versus displacement). Through a spectral analysis using a FFT (Fast Fourier Transform) the others modes of frequencies in the response are also captured. Figures 1a and 1b show the dynamical responses of the system governed by ODE in Eq. (5) in terms of the time series for the displacement and velocity, the phase diagrams and the Fourier spectra for two sets of parameters $\beta$ and $\varepsilon$. In Fig. 1a it is seen a typical response nearly nonlinear a high damping factor and frequency of excitation. Actually the solution is harmonic with double period (two modes) as shown in the Fourier spectrum of the signal. The phase diagram has a shape approximately circular that is a characteristic of a weak nonlinear system. In contrast, the plots in Fig. 1b for high values of the amplitude of excitation and of the nonlinear parameter $\varepsilon$ show a quite chaotic behavior of the response. In this extreme case, the phase diagram shape indicates the

existence of several freedom degree of vibrations that appear clearly as a continuous distributions of modes in the power spectrum of the response.

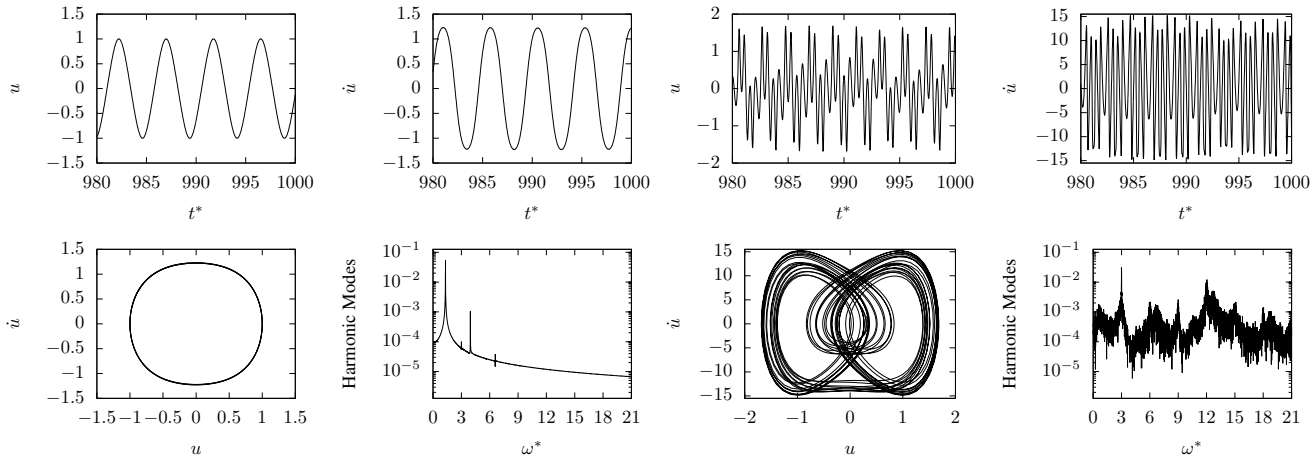


(a) (b)

Figure 1: Space signal, velocity signal, phase diagram and amplitude frequency specter for the nonlinear harmonic oscillator with (a) $\beta = 0.01$ and $\varepsilon = 1$; (b) $\beta = 100$ and $\varepsilon = 100$.

This preliminary analysis motivates us to say that concentrated models are a good starting point to construct more realistic theoretical models in the study of dynamic response of conductor cables undergoing harmonic or eolian excitation. In addition, real conductor cables can present nonlinear behavior due to its own internal structure of interwoven wire, sometimes made of different materials.

## 3. Experimental procedures

The experimental data in this work were collected after carrying out cable test in the Fatigue and Structural Integrity of Conductor Cables Laboratory at the University of Brasília. Figure 2 presents a sketch of the experimental test bench available in the same laboratory. In the laboratory the main focus is the study of fatigue from the maximum permissible vertical displacement that the peak of the cable anti-knot can reach (Kalombo *et al.*, 2016).

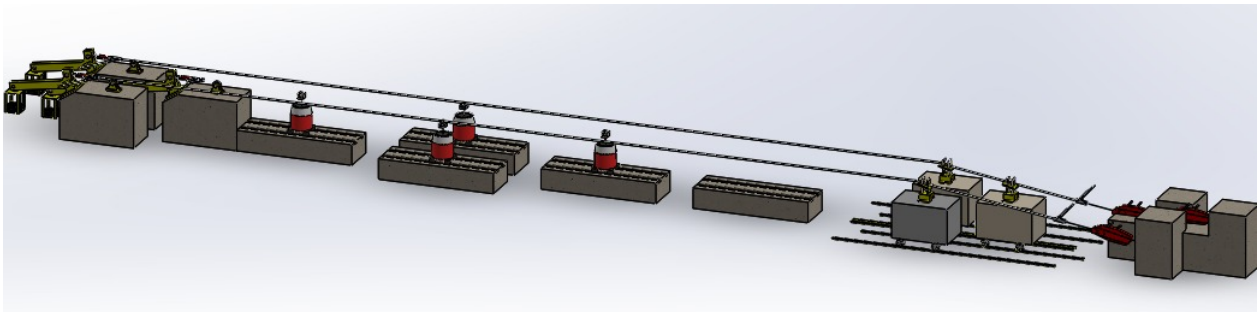

Figure 2: Cable test bench available in the Fatigue and Structural Integrity of Conductor Cables Laboratory at the University of Brasília - Brazil.

The conductor cable used in the experiments was the AAAC type (All Aluminum Alloy Conductors) 1120 fixed by CGS clamps (Cushion-Grip Suspension) as illustrated in Fig. 2. In the present work, which has a dynamic analysis character of the oscillation in cables, the acceleration data were collected over time in the accelerometers fixed in different positions of the cable.

By numerical integration, these data were converted into velocity and displacement data, which in turn were used to obtain displacement and velocity signals over time, at points on the cable. Such data were collected by four accelerometers placed close to a fixed end of the cable, so that the last accelerometer was at the peak of the anti-knot. The displacement between accelerometers change with the tension applied in the cable.

The experimental procedure evaluates the dynamic stress in the conductor cable form the vertical displacement $Y_b$ of a point on the cable located 89 mm from the suspension clamp, i.e. the point at which the accelerometer 1 is positioned. This distance is a technical specification established by the IEEE, Chan *et al.* (2009) and Liu *et al.* (2011), so that the relationship between cable vibration and the degree of fatigue can be reliable. Thus, the displacement of accelerometer 1

was taken as the input for the test, since the oscillation caused in the cable was intended to reach a desired displacement at that point.

With the displacement and velocity signals, phase diagrams and fast Fourier transforms of the displacement signals can be generated to finally adjust the concentrated model so that the experimental data could be fitted by the theoretical model examined in this work.

### 3.1 Experimental results

The responses observed at the experimental results were basically linear, as suggested by the plots of the signal time series, phase diagrams and power spectrum presented in Fig. 3. The results were obtained for conditions of two traction in the cable and an amplitude of 0.2 in the accelerometer 1. The scenario of linear response always occurred, because the experiments in that specific lab are restricted to investigate fatigue of cable in several cycle with harmonic excitation at a sufficient low amplitude.

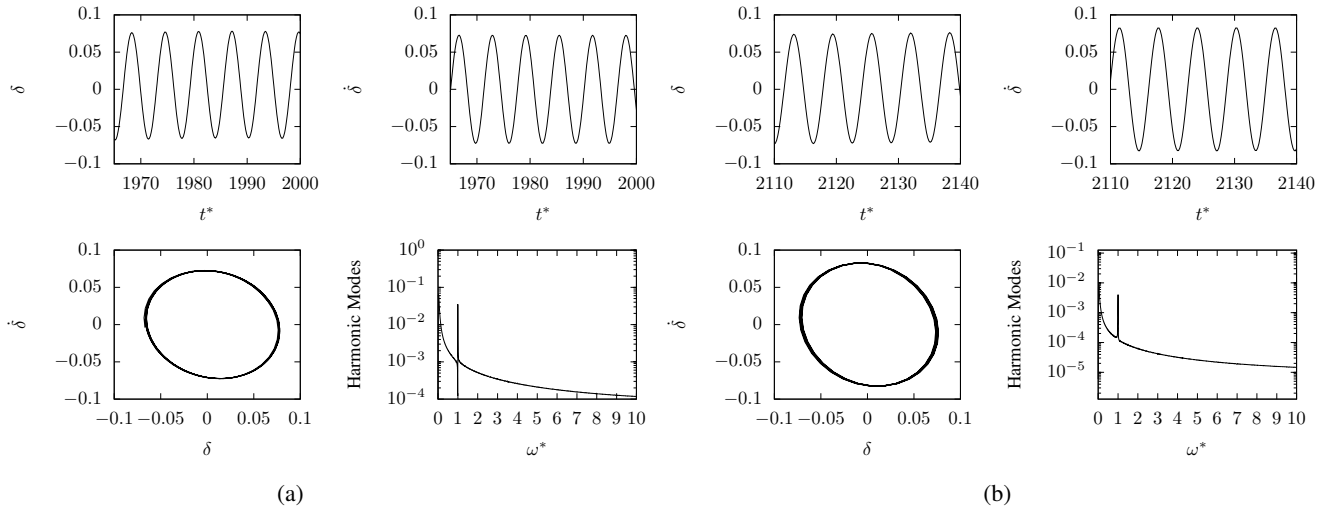


(a) (b)

Figure 3: Experimental results for (a) 15% stress of the rupture limit applied on the cable and an amplitude of 0.2 mm on the accelerometer 1; (b) 25% stress of the rupture limit applied on the cable and an amplitude of 0.2 mm on the accelerometer 1.

Now, in order to compare the theoretical predictions with observations, the experimental results were made nondimensional. The nondimensional vertical displacement $\delta$ is the ratio between the displacement in meters and the cable nominal diameter of 23.53 mm; the nondimensional time $t^*$ is the product between the time in seconds and the natural frequency at which the cable was excited, which in turn varied for each stress and excitation amplitude; the nondimensional velocity $\dot{\delta}$ denotes the ratio between the velocity given in m/s and the product between the nominal diameter of the cable and its natural frequency.

### 3.2 Comparison between the nonlinear harmonic model and the experimental results

The concentrated model is given by the Eq. (5), attending the initial conditions: $u(0) = 0$ and $\dot{u}(0) = 0$, those correspond the real situation of a cable at rest and at in the equilibrium position (i.e. null displacement) at the initial time. The parameters $\zeta$, $\beta$, $\omega^*$ and $\varepsilon$ were adjusted according to the experimental conditions and cable properties. The excitation amplitude $\beta$ was made equal to the control amplitude of accelerometer 1 (see section 3) nondimensional by the nominal diameter of the cable. The nondimensional excitation frequency $\omega^*$ was considered the unit, since the cable is excited at its natural frequency. The nondimensional parameter $\varepsilon$ (Eq. 6) corresponds to a nonlinearity attributed to the elastic restitution coefficient, as shown in the Eq. (2). This parameter depends on another one denoted $a$, which must be adjusted, since it was not measured experimentally. The coefficient $A$, in turn, given in meters, corresponds to the characteristic parameter used to make nondimensional the vertical displacement, which in this case was the nominal diameter of the cable. Finally, the elastic coefficient $k$ was obtained as follows: by the stiffness of the cable $EI$ (2,586 x $10^7$ Nmm$^2$), a value of $E$ was obtained considering the moment of inertia as the of circular section with the nominal diameter of the cable ($I = \pi d_n^4/64$); the value of $k$ was finally obtained by multiplying $E$ also by the nominal diameter of the cable, as it corresponds to the coefficient of restitution of a cross section, resulting in a value of 2,82 x $10^4$ N/mm$^2$.

Now, substituting $k$ for this result and $A$ for the cable diameter, we obtained that $\varepsilon = 0.025a$, where $a$ would be the model's adjustment parameter along with the damping $\zeta$, also experimentally indeterminate. Therefore in th present work, the damping factor and the parameter $a$ were adjusted according to the experimental results. These parameters were

calibrated for the smallest nondimensional excitation amplitude $\beta$ and, when a satisfactory value was obtained, results were than generated considering several amplitudes of excitation.

The damping was adjusted to an underdamping regime with $\zeta = 0.05$, which is reasonable given that the damping imposed by the air on the cable is very small. The nonlinear parameter $a = 4\ \text{N/m}^3$ was adjusted so that $\varepsilon$ resulted in 0.1.

Finally, in order to show the comparisons between the theoretical predictions and the data from the cable tests, we present in Fig. 4 plots for the maximum cable displacement achieved by the displacement signal as a function of the imposed amplitude of the excitation. Actually, we have considered the control amplitude in accelerometer 1 as the excitation amplitude, since it was considered an input of the dynamical cable system investigated here. Figures 4a, 4b and 4c shows the maximum displacement as a function of the excitation amplitude for three different traction applied to the cable during the experimental runs.

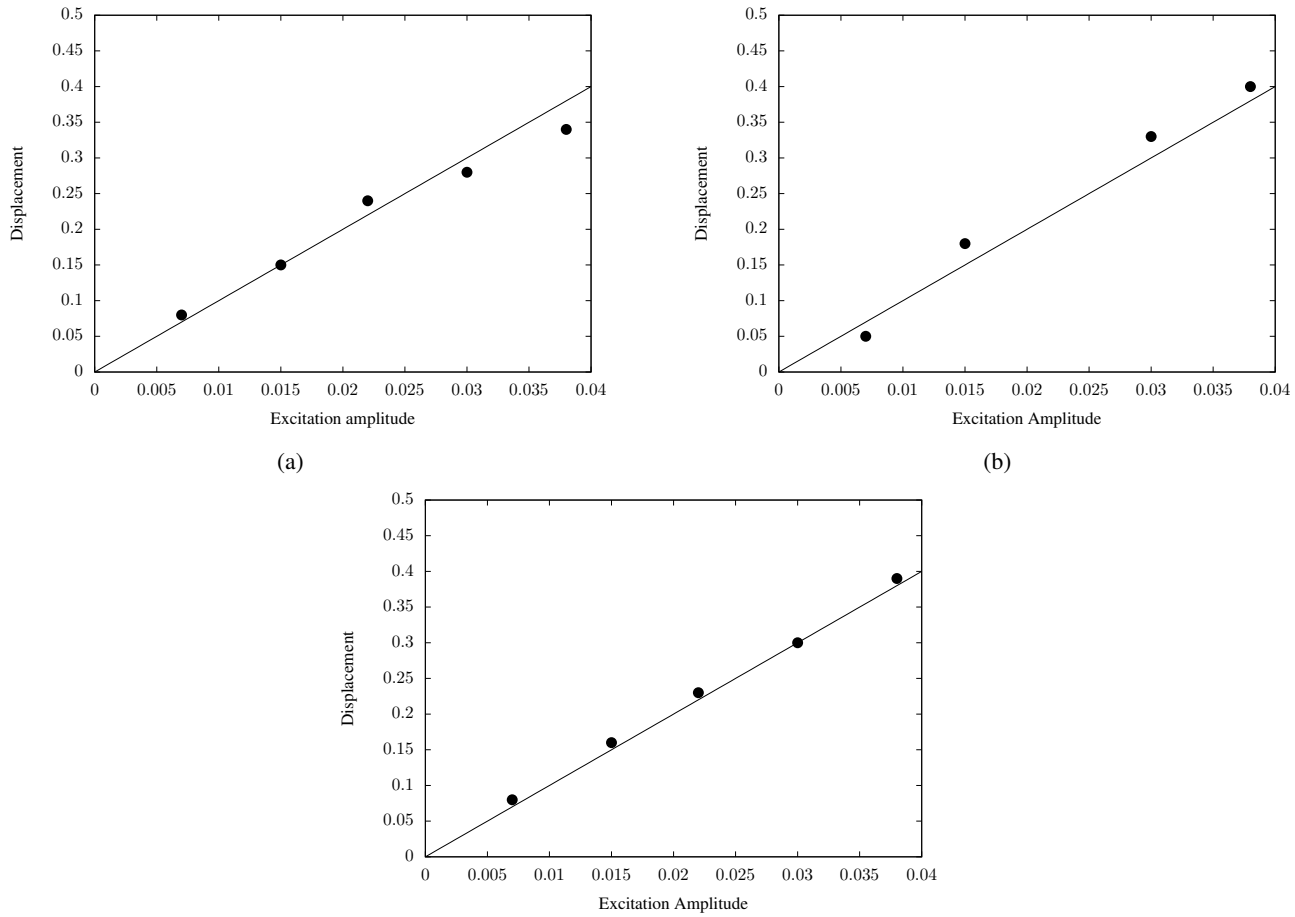


Figure 4: Comparison between the theoretical model of this work (full line) and the experimental results (•) for (a) a 15% stress of the rupture limit applied to the cable, (b) for a 20% stress of the rupture limit and (c) for a 25% stress of the rupture limit. The associated error bars with the experimental data were in average less than 5%.

For the three cases of applied traction, the theoretical results predicted by the concentrated model persists invariant, since the concentrated theory does not capture the influence of different traction applied in the cable. As shown in Fig. 4 only the experimental response it is seen to vary slightly as the cable traction change. However the results presented in Fig. 4 indicates that the maximum displacement in the cable response is always proportional to the amplitude of the excitation, regardless of the applied traction, basically having the same linear behavior.

A remarkable point here was to have observed a very similar behavior between the experimental data and the theoretical predictions even based on a concentrated model. As shown in all plots of Fig. 4 the experimental points are very well fitted by the theory, with a small difference that does not exceed 5% for all applied traction in the cable.

In general, we have observed a very good agreement between the theoretical predictions of our model and the experimental data from typical test of undergoing harmonic forcing of low amplitude. The applied traction on the cable demonstrated to have only a secondary effect in a linear regime of oscillations.

## 4. Concentrated model of a cylindrical cable

The model presented below consists of a cylinder, with mass $m$, subjected to a transverse flow of velocity $U$, and held at the ends by four springs of equal masses and the same elastic coefficient ($k_{spring}$), as shown in Fig. 5a. Springs provide the system elasticity while damping is an intrinsic feature. As the springs behave in parallel, there is an equivalent elastic coefficient $k_{eq}$ and, therefore, the entire system can be reduced to one of the spring mass type, with an equivalent mass like the model diagram shown in Fig. 5b.

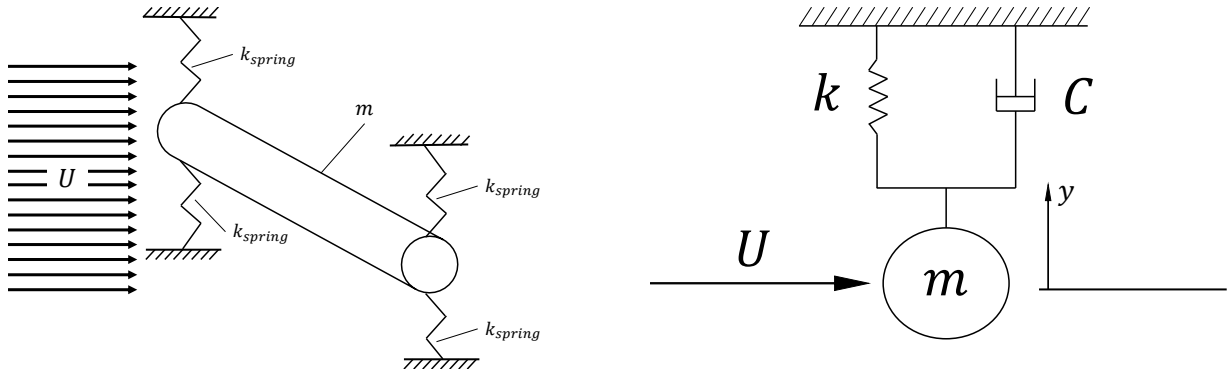


(a) (b)

Figure 5: (a) Concentrated model of a cylinder suspended by four springs and under a laminar flow with velocity $U$. (b) Equivalent spring-mass diagram model.

Now, by a balance of forces of the free-body diagram (Fig. 5a), we have that the equation for the equivalent dynamical cable system is given by:

$$m\ddot{y} + C\dot{y} + ky = F(t). \tag{7}$$

The external forcing $F(t)$ is of the harmonic type transversal to the flow, arising from the alternating formation of vortices downstream of the cylinder. Based on the work of Diana and Falco (1971), the following equation is proposed for this force:

$$F(t) = F_0 \cos(\Omega t), \tag{8}$$

where $\Omega$ is a frequency excitation and $F_0$ is a lift force expressed by

$$F_0 = \rho d U^2 C_L. \tag{9}$$

Here $\rho$ is the specific mass of the working fluid, in this case air, $d$ is the radius of the cylinder's cross section, $U$ is the velocity of the undisturbed flow and $C_L$ is the lift coefficient proposed by Oliveira and Freire (1994), which in turn is expressed, in nondimensional terms by

$$C_L(t^*) = \alpha_0 + \alpha_1 \delta(t^*) + \alpha_2 \delta^2(t^*). \tag{10}$$

The polynomial coefficients are determined by fitting experimental data, while $\delta$ and $t^*$ are, respectively, the nondimensional transverse displacement and the nondimensional time scale, defined as

$$\delta = \frac{y}{d}; \quad t^* = \omega_n t, \tag{11}$$

being $\omega_n$ the natural frequency of the cable system.

The final nondimensional governing equation, substituting the lift-coefficient by Eq. (10), results in

$$\frac{d^2\delta}{dt^{*2}} + 2\zeta \frac{d\delta}{dt^*} + \delta = \varepsilon \omega_r^2 (\alpha_0 + \alpha_1 \delta(t^*) + \alpha_2 \delta^2(t^*)) \cos(\omega t^*), \tag{12}$$

where $\varepsilon$ is a mass balance parameter defined as

$$\varepsilon = \frac{\rho_{fluid}}{\rho_{cylinder}} \frac{1}{\pi} \frac{1}{Sh^2}. \tag{13}$$

As this is a theoretical model to approximate the phenomenon of oscillating cables, the cylinder in question must be made of aluminum or steel, whereas the fluid in this case is air. Therefore, $\rho_{fluid} \ll \rho_{cylinder}$, leading to $\varepsilon \ll 1$. In this asymptotic limit we shall propose one analytical solution of Eq. (12) by using a regular perturbation method as described in Hinch (1991). Furthermore, using the properties of the cable tested in the experiments, it is possible to check the real value of $\varepsilon$. Therefore, using $\rho_{ar} = 1.225$ g/m$^3$ and evaluating Strouhal number given in Eq. (1). Here $\omega_s$ corresponds to a natural frequency of the conductor used in the experiment, $d$ is assumed as being the nominal radius of the cable cross section and a typical $U$ of the experiments is 10 m/s, that corresponds to the value of limit wind speed vibrations occur. Under these conditions the value of $\varepsilon$ was found to be $10^{-4} \ll 1$.

### 4.1 An asymptotic solution

Now, we use a regular perturbation method to solve analytically the nonlinear Eq. (12) in the limit in which $\varepsilon << 1$. Therefore, the following asymptotic expansion for $\delta$ is considered:

$$\delta = \delta_0 + \delta_1\varepsilon + \delta_2\varepsilon^2 + \cdots = \sum_{n=0}^{\infty} \delta_n \varepsilon^n. \tag{14}$$

Substituting Eq. (14) in the Eq. (12), is possible reach the ODE's system up to $O(\varepsilon^2)$:

$$\begin{cases} \ddot{\delta_0} + 2\zeta\dot{\delta_0} + \delta_0 = 0, \\ \ddot{\delta_1} + 2\zeta\dot{\delta_1} + \delta_1 = (\alpha_0 + \alpha_1\delta_0 + \alpha_2\delta_0^2)\omega_r^2\cos(\omega t^*), \\ \ddot{\delta_2} + 2\zeta\dot{\delta_2} + \delta_2 = (\alpha_1\delta_1 + \alpha_2 2\delta_1\delta_0)\omega_r^2\cos(\omega t^*). \end{cases} \tag{15}$$

Solving the $O(1)$ equation for $\delta_0$ three distinct solutions must be considered for each damping case. Thus, for the under-damped case ($\zeta < 1$), the solution is given by

$$\delta_0(t^*) = e^{-\zeta t^*}\left[A_1\sin(\sqrt{1-\zeta^2}t^*) + A_2\cos(\sqrt{1-\zeta^2}t^*)\right]. \tag{16}$$

In the damped critical case ($\zeta = 1$)

$$\delta_0(t^*) = A_1 e^{-t^*} + A_2 t^* e^{-t^*}. \tag{17}$$

And finally, for the super-damped case ($\zeta > 1$), the solution is given by:

$$\delta_0(t^*) = e^{-\zeta t^*}\left(A_1 e^{-\sqrt{\zeta^2-1}t^*} + A_2 e^{\sqrt{\zeta^2-1}t^*}\right), \tag{18}$$

where the coefficients $A_1$ and $A_2$ are obtained from the initial conditions, which are $\delta(0) = 0$ and $\dot{\delta}(0) = 0$, implying that these constants are null, and consequently leading to the trivial solution for $\delta_0 = 0$.

With the trivial solution for the $O(1)$ solution $\delta_0$, the system of ODE's equation given in (15) is reduced for:

$$\begin{cases} \ddot{\delta_1} + 2\zeta\dot{\delta_1} + \delta_1 = \alpha_0\omega_r^2\cos(\omega t^*), \\ \ddot{\delta_2} + 2\zeta\dot{\delta_2} + \delta_2 = \alpha_1\delta_1\omega_r^2\cos(\omega t^*), \end{cases} \tag{19}$$

whose solutions are separated into a homogeneous and a steady contributions. The homogeneous part of the solution may be given by one of the solutions presented in Eq. (16), Eq. (17) and Eq. (18), depending on the type of damping involved in the cable dynamics. On the other hand the steady solution is found by the well-known parameter variation method. The calculations were performed by using the software Maple. The results of the integration of Eq. (19) are depicted in Fig. 6 in terms of time series response, phase diagram and Fourier spectrum for the three cases of damping.

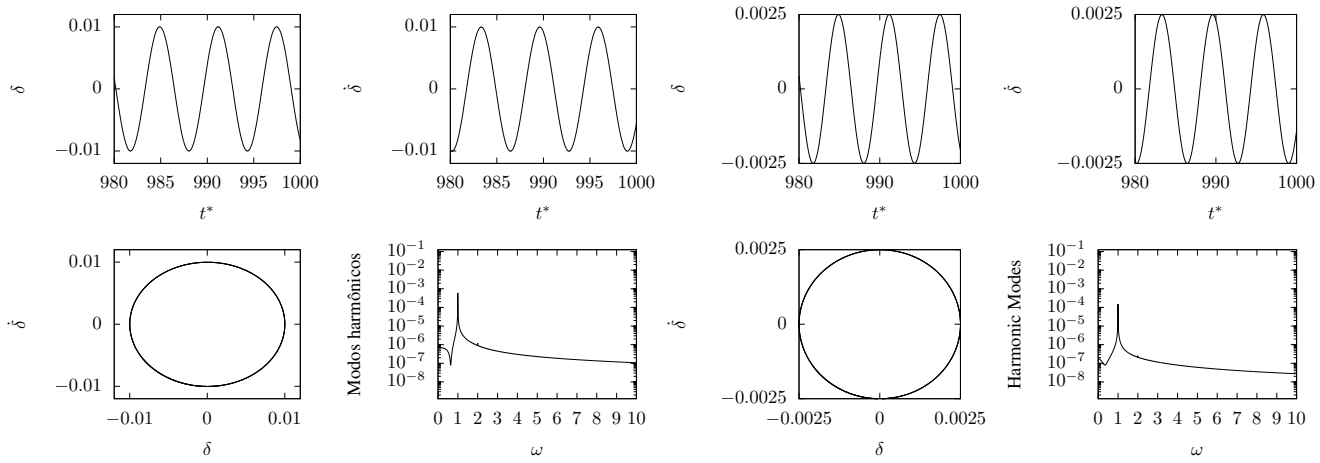


(a) (b)

Figure 6: The concentrated model response with wind excitation for (a) $\varepsilon = 0.01$ and under-dumped regimen; (b) $\varepsilon = 0.01$ and super-damped regime.

It is seen form Fig 6a and 6b that the steady solution for the concentrated model for $\varepsilon << 1$ is a simple harmonic mode, despite the nonlinear excitation of the eolian type. Based on this result, we could use the lower order of the polynomial function for the lift coefficient (Eq. 10) in order to check if would exist a similar solution to the nonlinear harmonic oscillator discussed in section 2. The idea here is also to incorporate in the concentrated cylinder model a nonlinear term associated with a more complex elasticity (i.e. a nonlinear elastic force) such as must occur in the case of real cables.

For this end, a comparative study of the solutions of the concentrated cylinder model with excitation taking the forms of a polynomial of degree 0, 1, 2 and 3 was performed, for values of $\varepsilon$ ranging from zero to 1. The main goal is to find for which values of the parameter $\varepsilon$, the solution even for different degree of excitation nonlinearity still converges.

The second order nonlinear differential for arbitrary $\varepsilon$ (e.g. $O(1)$) Eq. (12) was integrated numerically by using a fourth-order Runge-Kutta algorithm with a typical time step equal to 0.01. The asymptotic solution for small $\varepsilon$ with the full excitation presented in section 4 was used to verify the numerical solution at small values of the same parameter.

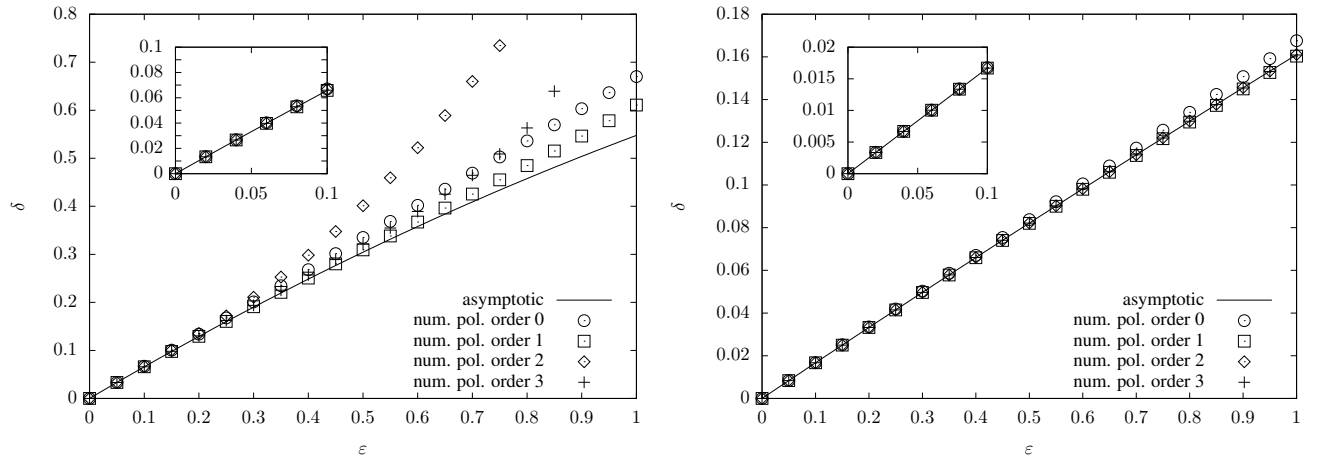


(a) (b)

Figure 7: Comparison between the asymptotic and numerical solutions for a fixed nondimensional time unit around 50. (a) Under-damping and (b) super-damping.

Despite the different convergence situations, what is remarkable in the damping cases presented in Fig. 7 is the convergence of all solution independent of the nonlinearity degree of excitation, for values of $\varepsilon \ll 1$. This corresponds exactly the case of real cables or cylinders undergoing an eolian excitation. Therefore, since that $\varepsilon$ is small in the real case, we can compute the wind excitation just with the lower order polynomial involving the coefficient $\alpha_0$ and use the concentrated model of the nonlinear harmonic without the term involving nonlinear elasticity. From a general point of view, the nonlinear oscillation model presented in section 2 and the concentrated cylindrical cable model showed in section 4 can be interpreted as a concentrated spring-mass damper model on which certain elements and conditions are added in order to generate results that better represent what we really intended to explore in the dynamical system.

## 5. Cable vibrating model

Considering the free-body diagram in Fig. 8, the governing equation of the vibratory movement of a conductor cable can be determined by force balance, under the following assumptions:

- The particles that make up the cable move only in the $y$ direction (transverse vibration);
- The conduction cable has constant transversal section, that is, its inertia moment $I$ does not vary in the $x$ direction nor with time $t$;
- The cable's modulus of elasticity $E$ is constant and, like $I$, it does not vary in time or space $x$;
- The horizontal force $T$ is the same force applied to the cable in its ends when they are pinned to poles;
- It is reasonable to assume the $T$ force invariant over time;
- The cable linear density is homogeneous, that is, $\boldsymbol{\nabla}\gamma = \mathbf{0}$.

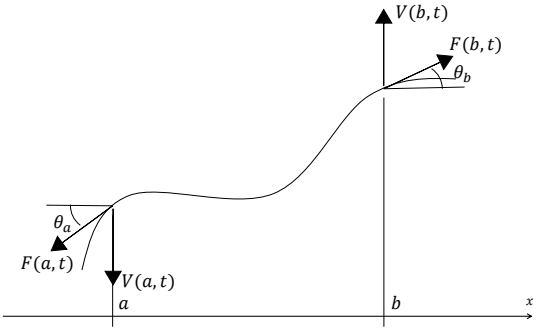


Figure 8: Free-body diagram of a typical vibrating cable.

It is well-known that the governing equation of a vibrating string is given by (de Figueiredo, 2000):

$$\gamma \frac{\partial^2 y}{\partial t^2} = T \frac{\partial^2 y}{\partial x^2} + F_{ext}, \tag{20}$$

where $F_{ext}$ is the external forces acting over the string, nevertheless a conductor cable presents a flectional resistance. Under this condition, the sum of the external forces considered in the balance to get the governing equation takes into account the vertical shear forces $V(x,t)$. Thus, the governing equation for a cable developing a vibratory motion is given by:

$$EI \frac{\partial^4 y}{\partial x^4}(x,t) - T \frac{\partial^2 y}{\partial x^2}(x,t) + \gamma(x) \frac{\partial^2 y}{\partial t^2}(x,t) = F_{ext}(x,y,t). \tag{21}$$

Now, to make Eq. (21) nondimensional, the same characteristics scales used for the cylinder model are also considered here. However, adding one more to the $x$ position along the cable, which would be $x^* = x/L$, where $L$ is the longitudinal length. So, after few algebraic manipulations, we obtain the following equation in terms of nondimensional quantities:

$$\frac{EI}{L^2 T} \frac{\partial^4 \delta}{\partial x^{*4}}(x^*,t^*) - \frac{\partial^2 \delta}{\partial x^{*2}}(x^*,t^*) + \frac{\gamma \omega_n^2 L^2}{T} \frac{\partial^2 \delta}{\partial t^{*2}}(x,t) = \frac{L^2}{aT} F_{ext}(x^*,t^*). \tag{22}$$

It should be important to note that the inertia moment parameter $EI/L^2T$ that multiplies the fourth derivative on the left hand side of Eq. (22) is very small. Therefore, it is possible to neglected this contribution in Eq. (22) as compared with the others contributions which dominate the cable oscillatory motion. In real applications, the cable length has an order of $10^2$ m, the traction force on the cable pins has an order of $10^4$ N, the elasticity modulus $E$ of a cable made mostly of aluminum has an order of $10^{10}$ Pa, and for last the cable inertia moment $I$ has an order of $10^{-8}$ m$^4$, resulting in a inertia moment parameter of order $10^{-6}$.

Now, considering the previous definition of string propagation velocity $c = \sqrt{T/\gamma}$, is possible define a nondimensional propagation velocity as:

$$c^* = \frac{c}{L\omega_n}. \tag{23}$$

Under these conditions, Eq. (22) is reduced to:

$$\frac{\partial^2 \delta}{\partial t^{*2}} - c^{*2} \frac{\partial^2 \delta}{\partial x^{*2}} = A_0 F_{ext}(x^*, t^*). \tag{24}$$

In addition, considering the contribution of a nondimensional self-damping (Diana *et al.*, 2000) proportional do velocity $\partial\delta/\partial t$, we have

$$Ca\omega_n \frac{\partial \delta}{\partial t^*}(x^*, t^*), \tag{25}$$

where $C$ is a self-damping coefficient. Additionally, a restoring force typically proportional to displacement $\delta$ takes the form:

$$ka\delta(x^*, t^*). \tag{26}$$

Here $k$ is the elastic coefficient of the cable. Finally, including the contributions (25) and (26) on the right hand side of Eq. (24), we obtain a complete form of the cable governing equation in terms of nondimensional variables:

$$\frac{\partial^2 \delta}{\partial t^{*2}} - c^{*2} \frac{\partial^2 \delta}{\partial x^{*2}} = A_0 F_{exc}(x^*, t^*) + 2Z \frac{\partial \delta}{\partial t^*}(x^*, t^*) + K\delta(x^*, t^*), \tag{27}$$

where $2Z = 2C/\gamma\omega_n$ and $K = k/\gamma\omega_n^2$. It should be important to note that the forcing term $A_0 F_{exc}(x^*, t^*)$ can be a harmonic function as proposed in the model of a nonlinear harmonic oscillator discussed in section 2 of this work or a real excitation produced by wind effect such as used in the concentrated model of a cylindrical cable (see section 4). This model describing the spatial-temporal dependence of the cable displacement is physically consistent to the simplified model of concentrated cable if the traction on the cable is sufficiently small. In this limit of small traction the second term on the left hand side of Eq. (27) becomes very small and may be neglected. Consequently, under this asymptotic limit of $c^* \ll 1$ the full model giving by Eq. (27) reduces to a concentrate model presented in section 2. In a future work we plan to solve Eq. (27) numerically for different possibility of real boundary conditions and compare the results for small $c^*$ with those obtained using a concentrated model.

## 6. CONCLUSIONS

We have presented a dynamic analysis for the nonlinear oscillator by using phase-space diagrams and amplitude-frequency plots, and by exploring the chaotic response of the system for nonlinear regimes with high amplitudes of excitation. Experiments with a real transmission cable undergoing harmonic oscillations were carried out in order to measure the time-response at different longitudinal positions. We have adjusted the system parameters of the theoretical model for the real values of the experiments and the nonlinear harmonic oscillator successfully have fitted the experimental data. When the nondimensional physical parameter of the concentrated model of a cylindrical cable system is much smaller than unity, a perturbation method was used to provide an asymptotic solution for the prototype cable displacement. An excellent agreement was observed between the asymptotic and numerical solutions based on a standard Runge-Kutta algorithm. For appropriate condition of damping and excitation, and after few manipulations, the concentrated cylindrical cable model was seen to be equivalent to the nonlinear harmonic oscillator model. Finally, the vibrating motion of the prototype cylindrical cable was examined. From a scaling analysis of the nondimensional second order partial differential governing equation of the cable motion in space-time, the equivalence and consistency between the continuous and the concentrated models were demonstrated. We have shown that for small values of tensions applied to the cable, the wave propagation velocity is sufficiently small, and consequently the space second derivative along the length of the cable is only a weak contribution, resulting in a concentrated mass-spring-damper system.

## 7. ACKNOWLEDGEMENTS

The authors are grateful to the entire team at the Fatigue and Power Cable Structural Integrity Laboratory in the Department of Mechanical Engineering at University of Brasilia - Brazil for providing the experimental data used in the research. We also would like to thank the Brazilian National Council for Scientific and Technological Development - CNPq (Grants no. 310399/2020-3 and 421177/2018-7), the Foundation Support Research DF - FAPDF and the Coordination for the Improvement of Higher Education Personnel - CAPES DF (Grants no. 88887.605035/2021-00) for the financial support throughout the development of this work.

## 8. REFERENCES

Batchelor, G.K., 2000. *An Introduction to Fluid Dynamics*. Cambridge University Press, Cambridge.

Chan, J., Havard, D., Rawlins, C., Diana, G., Cloutier, L., Lilien, J.L., Hardy, C., Wang, J. and Goel, A., 2009. *EPRI Transmission Line Reference Book: wind-induced Conductor Motion.* EPRI, Palo Alto.

de Figueiredo, D.G., 2000. *Fourier analysis and partial differential equations (in portuguese).* Instituto de Matemática Pura e Aplicada - IMPA, Rio de Janeiro.

Den Hartog, J.P., 1972. *Vibrations in mechanical systems (in portuguese).* Editora Edgard Blücher Ltda, São Paulo.

Diana, G. and Falco, M., 1971. "On the forces transmitted to a vibrating cylinder by a blowing fluid". *Meccanica*, Vol. 6, No. 1, pp. 9–22.

Diana, G., Falco, M., Cigada, A. and Manenti, A., 2000. "On the measurement of overhead transmission lines conductor self-damping". *IEEE Transactions on Power Delivery*, Vol. 15, No. 1, pp. 285–292.

Guerard, S., Godard, B. and Lilien, J.L., 2011. "Aeolian vibrations on power-line conductors, evaluation of actual self damping". *IEEE Transactions on Power Delivery*, Vol. 26, No. 4, pp. 2118–2122.

Hinch, E.J., 1991. *Perturbation Methods*. Cambridge University Press, Cambridge.

Kalombo, R., Araújo, J., Ferreira, J., Da Silva, C., Alencar, R. and Capra, A., 2016. "Assessment of the fatigue failure of an all aluminium alloy cable (aaac) for a 230 kv transmission line in the center-west of brazil". *Engineering Failure Analysis*, Vol. 61, pp. 77–87.

Liu, S., Sun, N., Yin, Q., Qi, Y., Cao, D. and Zhang, L., 2011. "Study of new vibration suppression devices for application to ehv transmission line groundwires". *Energy Procedia*, Vol. 12, pp. 313–319.

Logan, J.D., 2013. *Applied mathematics*. John Wiley & Sons, Hoboken.

Oliveira, A.R. and Freire, D.G., 1994. "Dynamical modelling and analysis of aeolian vibrations of single conductors". *IEEE transactions on power delivery*, Vol. 9, No. 3, pp. 1685–1693.

## 9. RESPONSIBILITY NOTICE

The authors are solely responsible for the printed material included in this paper.